

## Article

# Structural, Magnetocaloric, and Magnetic Properties in Heusler Ni<sub>50</sub>Mn<sub>35</sub>In<sub>10</sub>X<sub>5</sub> (X = Ga, Fe and Al) Alloys

Tarek Bachagha <sup>1,2,\*</sup> , Ramki Chakaravarthy <sup>1</sup>, Wei Ren <sup>1</sup>, Joan Saurina <sup>2</sup>  and Joan-Josep Suñol <sup>2,\*</sup> 

<sup>1</sup> Physics Department, International Center of Quantum and Molecular Structures, Shanghai University, Shanghai 200444, China; chakaravarthy@shu.edu.cn (R.C.); renwei@shu.edu.cn (W.R.)

<sup>2</sup> Physics Department, Universitat de Girona, Campus Montilivi, 17071 Girona, Spain; joan.saurina@udg.edu

\* Correspondence: bachagha@shu.edu.cn (T.B.); joan josep.sunyo@udg.edu (J.-J.S.)

**Abstract:** The structural, magnetocaloric, and magnetic characteristics in Heusler Ni<sub>50</sub>Mn<sub>35</sub>In<sub>10</sub>X<sub>5</sub> (X = Ga, Fe, and Al) alloys were examined using X-ray diffraction and field-dependent magnetization measurements. All samples exhibited a mixture structure of cubic L2<sub>1</sub> and tetragonal L1<sub>0</sub> and underwent second-order magnetic transitions at T<sub>C</sub>(Al5) = 220 K, T<sub>C</sub>(Ga5) = 252 K, and T<sub>C</sub>(Fe5) = 298 K. The Ga5 alloy exhibited structural change as indicated by a thermal hysteresis that may be seen in the saturation magnetic field in the *M*(*T*) dependences. The transition at the T<sub>C</sub> point from a ferromagnetic to a paramagnetic state caused a drop in magnetization, supported by thermal hysteresis, at a low magnetic field (0.01 T). On the other hand, the Fe5 alloy presented a gradual decrease in magnetization with similar hysteresis behavior, also at a low magnetic field (0.01 T), whereas at 0.1 T of field, no features characteristic of this transition were detected. This could be due to a large difference in the metallic radius of Fe compared to that of In. Otherwise, magnetic investigations demonstrated that the replacement of In with Al may cause the structural transformation temperatures and T<sub>C</sub> to be shifted to low temperatures. The present results imply that the structural transformation temperatures and the transition itself are highly dependent on chemical composition. Furthermore, under a magnetic field change of 5 T, the maximum magnetic entropy changes of 0.6 J/kg K, 1.4 J/kg K, and 2.71 J/kg K for the Ga5, Fe5, and Al5 alloys, respectively, were determined by their T<sub>C</sub>. Refrigeration capacity values were found to be 25 J/kg, 74 J/kg, and 98 J/kg at μ<sub>0</sub>Δ*H* = 5 T. These ribbons are viable candidates for multifunctional applications due to their cheaper cost and their physical characteristics disclosed during the magnetostructural transition, which takes place close to the room temperature.

**Keywords:** Heusler alloys; magnetic transition; magnetocaloric effect; magnetic refrigerant materials



**Citation:** Bachagha, T.; Chakaravarthy, R.; Ren, W.; Saurina, J.; Suñol, J.-J. Structural, Magnetocaloric, and Magnetic Properties in Heusler Ni<sub>50</sub>Mn<sub>35</sub>In<sub>10</sub>X<sub>5</sub> (X = Ga, Fe and Al) Alloys. *Metals* **2023**, *13*, 1913. <https://doi.org/10.3390/met13121913>

Academic Editor: Cristian Ciobanu

Received: 10 October 2023

Revised: 2 November 2023

Accepted: 14 November 2023

Published: 21 November 2023



**Copyright:** © 2023 by the authors. Licensee MDPI, Basel, Switzerland. This article is an open access article distributed under the terms and conditions of the Creative Commons Attribution (CC BY) license (<https://creativecommons.org/licenses/by/4.0/>).

## 1. Introduction

Great consideration has been committed to the study of materials that show reasonable values of magnetic entropy change ( $\Delta S_M$ ) because they may be used as magnetic refrigerant materials at close to room temperature (RT) [1,2]. Heusler Ni–Mn–In alloys that undergo first-order temperature-instigated structural/martensitic transitions around RT have drawn interest because of their remarkable magneto-responsive properties, like the giant magnetocaloric effect (MCE), the shape memory effect (SM), exchange bias (EB), and large magnetoresistance (MR) [3–9]. One of their potential applications is in magnetic refrigeration systems, in which the application of an external magnetic field produces changes in the material associated with the extraction or transfer of heat.

In these alloys, the crystalline structure can change from austenite phase (cubic L2<sub>1</sub>) at high temperature to martensite phase (monoclinic 5M, orthorhombic, or tetragonal L1<sub>0</sub>) at low temperature, depending on the temperature and content. Typically, these alloys undergo a temperature martensitic transformation (reversible and hysteretic austenite to martensite) and a magnetic transformation (ferromagnetic (FM) to paramagnetic (PM)).

Thus, the four combinations can be obtained as a function of temperature and composition (austenite FM or PM, martensite FM or PM). Likewise, sometimes also relatively high-temperature atomic ordering (order–order or order–disorder) transformations or magnetic transformations (low-temperature superparamagnetism, spin glass) are found. For almost stoichiometric compositions, the magnetic coupling is ferromagnetic (FM), but for compositions rich in Mn, it is short-range antiferromagnetic (AFM) [10,11]. Thus, the magnetic transitions in these alloys have been reported at magnetostructural phase transition by Krenke et al. [11]. These materials may also be produced in a variety of shapes, such as 1D microwires, 2D ribbons, or 3D bulks, making them desirable candidates for multifunctional devices [12–14]. The structural martensitic transition for some Ni–Mn–In Heusler alloys was seen in Mn-based alloys, where both martensite and austenite phases display an FM order [15]. Moreover, in these alloys, the magnetization of austenite and its Curie temperature ( $T_C^A$ ) weakly change with the composition. On the other hand, the Curie temperature of martensite ( $T_C^M$ ) depends considerably on composition due to the exchange interactions strongly dependent on interatomic Mn–Mn distances [11]. The alloys  $Ni_{50}Mn_{50-x}In_x$  exhibited a considerable Curie temperature ( $T_C$ ) tumble from 310 K (for  $x = 20$ ) to 290 K (for  $x = 25$ ) [11]. As reported by Dubenko et al. [16], the doping of an additional element or a change in the chemical composition of Ni–Mn–In Heusler alloys can modify the hybridization of Ni(3d)–Mn(3d), the electron valence concentration ( $e/a$ ), and the interatomic distance of Mn–Mn. These variables may have an impact on phase transitions and related phenomena as well as the electronic band structure [17]. However, knowledge of the precise processes behind the intriguing behaviors of Heusler Ni–Mn–In alloys remains unsatisfactory. According to previous research, the concentration of X-doped components greatly affects: (a) the crystalline structure, (b) the magnetic and functional properties, and (c) the temperature interval of the transformations of Heusler Ni–Mn–In–X alloys [16–18]. Thus, understanding the processes responsible for these chemicals' particular behavior requires quaternary system research. In addition, due to the different metallic radius and electronic structure of X element compared to that of In, a change in characteristics can be expected.

In this work, we examine the impact of substituting the addition elements X for In on the structural, magnetic, and magnetocaloric characteristics of melt-spun ribbons of  $Ni_{50}Mn_{35}In_{10}X_5$  ( $X = Ga, Fe, \text{ or } Al$ ) Heusler alloys.

## 2. Materials and Methods

$Ni_{50}Mn_{35}In_{10}Ga_5$ ,  $Ni_{50}Mn_{35}In_{10}Fe_5$ , and  $Ni_{50}Mn_{35}In_{10}Al_5$  are the chemical formulas (atomic percentage) for the polycrystalline alloys, named Ga5, Fe5, and Al5, respectively, which were prepared by arc melting pure (99.98%) Ni, Mn, In, Al, Ga, and Fe elements (Sigma-Aldrich, St. Louis, MO, USA) in an argon environment and water-cooled copper crucible. For optimal homogeneity, the ingots were re-melted four times. An MSP10 melt-spinning machine (Edmund Bühler, Bodelshausen, Germany) with an argon atmosphere, a polished copper wheel rotating at a linear speed of 48 m/s, an orifice diameter of 0.5 mm, a 3 mm nozzle wheel distance, and an injection pressure of 500 mbar was used for producing the ribbons. The produced ribbons were between 1–2 mm wide and around 1–3 cm long.

Structures were examined using X-ray diffraction (XRD) on a Brüker D8 Advance diffractometer using Cu-K radiation. The MAUD program, which is based on the Rietveld technique, was used to computer-refine the XRD patterns [19]. The chemical compositions of the produced alloys were investigated using scanning electron microscopy (SEM, FEI Quanta 450) outfitted with energy-dispersive X-ray spectrometry.

The vibrating sample magnetometer (VSM) module of the PPMS DynaCool Cryogen-free System (Quantum Design, San Diego, CA, USA) was used to measure the isothermal and thermomagnetic magnetization curves up to a 5 T applied field. A magnetic field was applied in the direction the ribbon was rolling. The so-called “virgin effect” was removed during  $M(T)$  measurements by lowering the sample's temperature to 50 K in zero-field prior to each  $M(T)$  measurement, and then the curves for zero-field cooling (ZFC), field

cooling (FC), and field heating (FH) were methodically monitored [20]. In order to ensure the precision of  $\Delta S_M$  values, the so-called “loop procedure method” was used to gather the isothermal magnetization  $M(H)$  curves [21]. The isothermal magnetization measurements as a function of the applied magnetic field were used to compute the  $\Delta S_M$  around the  $T_C$ .

### 3. Results and Discussion

Figure 1 shows the Rietveld refinements of XRD patterns for the Ga5, Fe5, and Al5 alloys.

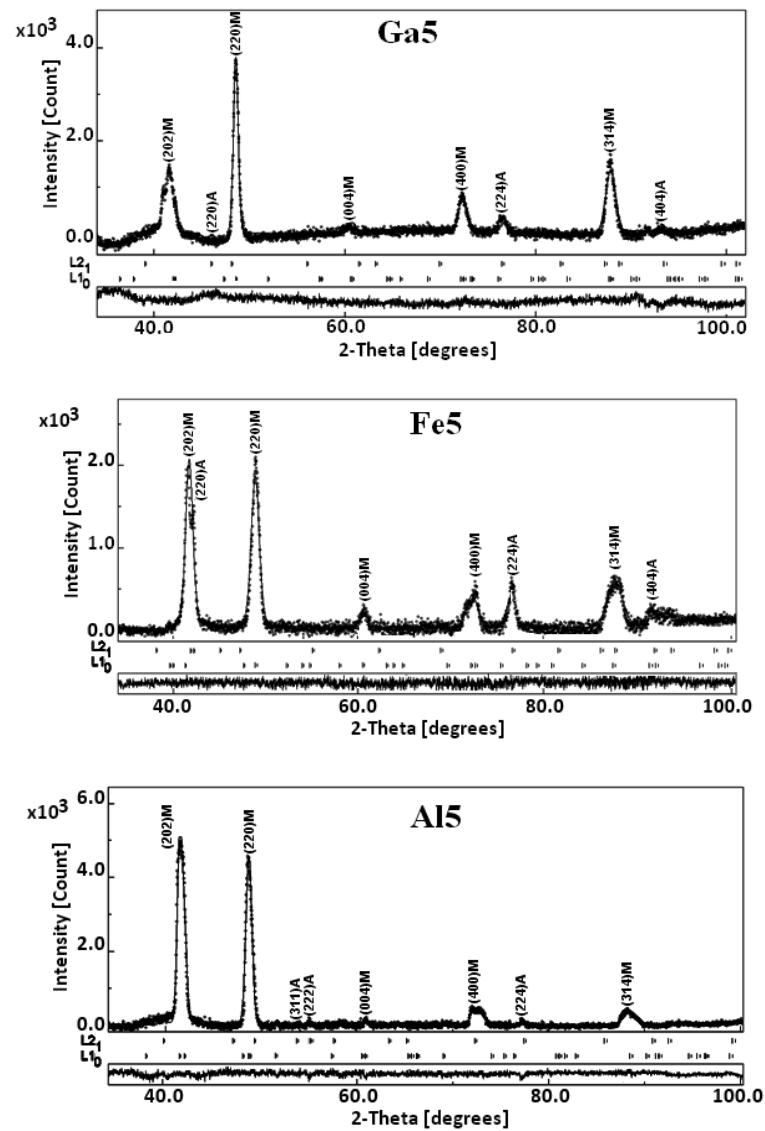


**Figure 1.** Rietveld refinement of the XRD patterns of the studied Ga5, Fe5, and Al5 alloys. The difference between the measured (dots) and calculated (line) patterns is shown below. The reliability factors are:  $GOF = 1.843$ ,  $R_{WP} (\%) = 7.127$ ,  $R_b (\%) = 4.885$ , and  $R_{exp} (\%) = 1.854$  in the case of the Ga5 sample;  $GOF = 1.771$ ,  $R_{WP} (\%) = 4.327$ ,  $R_b (\%) = 2.976$ , and  $R_{exp} (\%) = 2.442$  in the case of the Fe5 alloy; and  $GOF = 1.882$ ,  $R_{WP} (\%) = 4.936$ ,  $R_b (\%) = 3.427$ , and  $R_{exp} (\%) = 2.254$  for the Al5 sample.

As a result of the samples' rapid crystallization and growth dynamics during the melt-spinning process, the XRD patterns present intense and thin peak characteristics of a completely crystalline microstructure. A mixture of martensite (tetragonal  $L1_0$ , space group  $I4/mmm$ ) and austenite (cubic  $L2_1$ , space group  $Fm\bar{3}m$ ) phases was detected. The coexistence of the austenite and martensite phases is caused by the temperature-induced

first-order structural transition in both phases [22]. Such a mixed phase is typical in Ni–Mn–In Heusler alloys when the martensitic transition (MT) takes place close to RT [14,23]. Pathak et al. [10] reported the same structure. However, they only used a few peaks in the XRD pattern to determine this, which only provides limited information. Moreover, the XRD patterns of these ribbons are similar to that of bulk  $\text{Ni}_{50}\text{Mn}_{35}(\text{In}_{1-x}\text{Cr}_x)_{15}$  Heusler alloys in the phase coexistence region, exhibiting a magnetostructural transition near RT [24]. Since the metallic radius of Al (143 pm) is larger than that of Ga (135 pm) and even than that of Fe (126 pm) when substituting In (167 pm), a shift in peaks toward lower  $2\theta$  angles was detected, indicating an increase in the lattice parameters  $a$  and  $b$ , while seeing a decrease in the lattice parameter  $c$  [10]. XRD analysis confirmed that the minor addition (5 at.%) of an element modified the crystallographic structure. The lattice parameters were seen to be, in the case of the Fe5 alloy,  $a L2_1 = 5.998 \pm 0.003 \text{ \AA}$ ,  $a L1_0 = b L1_0 = 3.821 \pm 0.004 \text{ \AA}$ , and  $c L1_0 = 6.780 \pm 0.006 \text{ \AA}$  and, in the case of the Ga5 sample,  $a L2_1 = 6.061 \pm 0.003 \text{ \AA}$ ,  $a L1_0 = b L1_0 = 4.367 \pm 0.003 \text{ \AA}$ , and  $c L1_0 = 6.731 \pm 0.009 \text{ \AA}$ . Meanwhile, in the case of the Al5 alloy, the lattice parameters were seen to be  $a L2_1 = 6.066 \pm 0.005 \text{ \AA}$ ,  $a L1_0 = b L1_0 = 4.368 \pm 0.001 \text{ \AA}$ , and  $c L1_0 = 6.728 \pm 0.003 \text{ \AA}$ . These parameters are in great congruity with those of close chemical compositions, and recently detailed for Heusler  $\text{Ni}_{50-x}\text{Co}_x\text{Mn}_{32-y}\text{Fe}_y\text{Ga}_{18}$  and  $\text{Ni}_{50}\text{Mn}_{35}\text{In}_{15-x}\text{Bi}_x$  alloys [10,22].

Figure 2 displays the tetragonal  $L1_0$  and cubic  $L2_1$  crystal structures regarding the elements' sites. The stoichiometric Heusler alloys are ternary alloys with an atomic composition  $X_{50}Y_{25}Z_{25}$ . The Heusler alloys usually produced are off-stoichiometric, searching for an optimization of: (a) the functional response and (b) the temperature interval of the transformations. In our study, Ni occupies the X sites (red), Mn the Y sites (green), and in Z sites (blue) are expected the excess Mn and In, Fe, Ga, or Al. From the  $L2_1$  phase, the face-centered tetragonal  $L1_0$  structure is formed by distorting the cubic lattice built without modulation. All ribbons' creation of the martensite  $L1_0$  phase can be connected to a high level of internal stresses and structural defects as a result of the melt's quick solidification, which leads to quick crystallization. Additionally, the non-modulated and modulated martensite can have various structural variations depending on the production method and chemical composition. Indeed, the results obtained in our alloys for the coexistence of the cubic  $L2_1$  and tetragonal  $L1_0$  structures are comparable to those reported in  $\text{Ni}_{50}\text{Mn}_{35}\text{In}_{15-x}\text{Bi}_x$  ribbons by Aryal et al. [22].

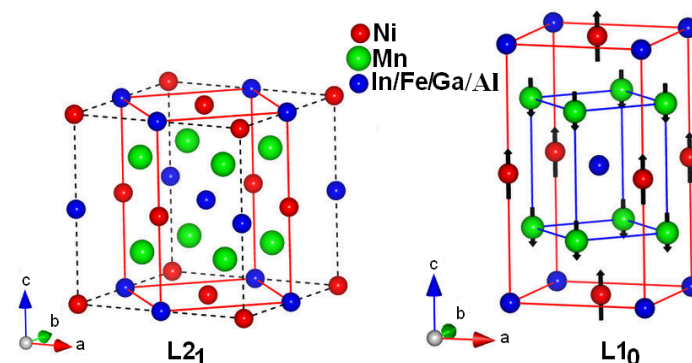


**Figure 2.** Illustration of cubic  $L2_1$  and tetragonal  $L1_0$  crystal structures ( $a$ ,  $b$ ,  $c$  unit vectors).

Figure 3 presents the micrographs relating to the wheel surface of the ribbons. The austenite  $L2_1$  appears in the ribbon plane as an equiaxed form, despite the fact that the martensite  $L1_0$  is in plate shape and the martensite plates provided the semi-parallel between plate interfaces. These ribbons quickly split along the direction opposite the ribbon plane because they are mechanically weak. EDX microanalysis was collected to assess for sample homogeneity. The compositions of the studied alloys are listed as follows: 50.1at.%Ni, 35.9at.%Mn, 9.2at.%In, 4.8at.%Ga; 51.6at.%Ni, 34.8at.%Mn, 8.9at.%In, 4.7at.%Fe; and 52.3at.%Ni, 33.7at.%Mn, 9.4at.%In, 4.6at.%Al. For all ribbons, the deviations in the

compositions were close to 0.05%. The compositional analysis revealed that the nominal and experimental compositions of the as-spun ribbons were quite similar.

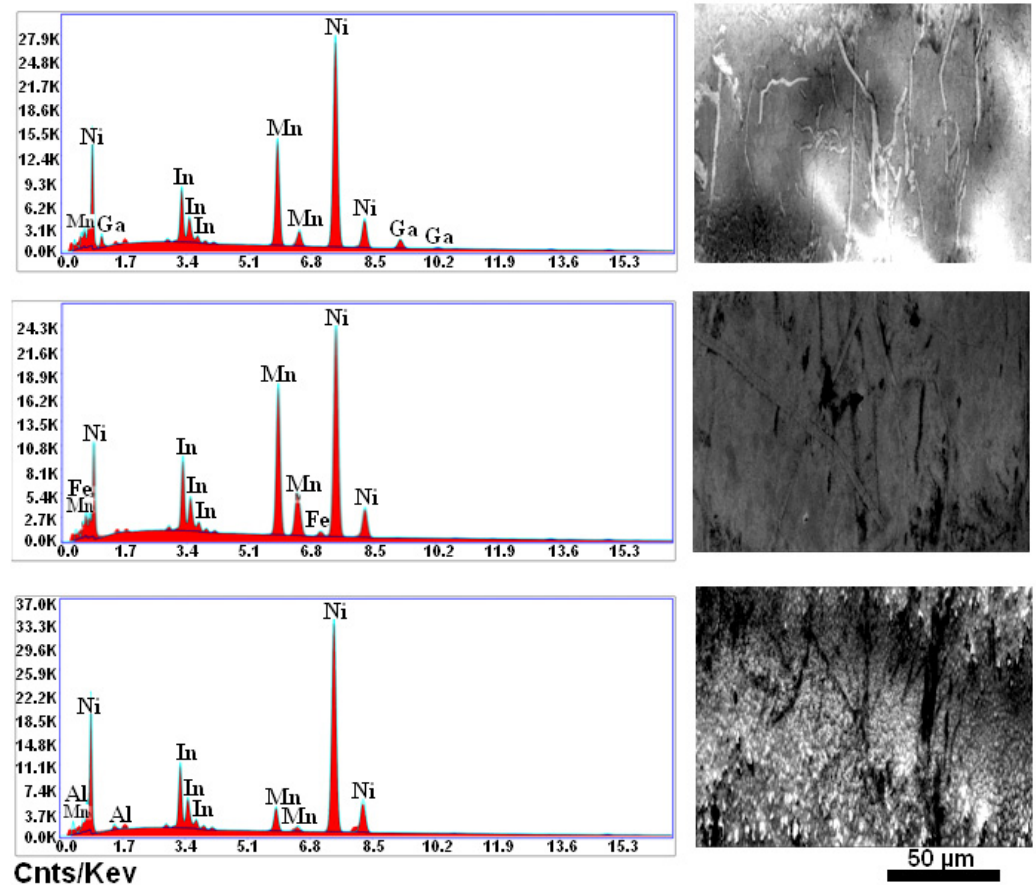
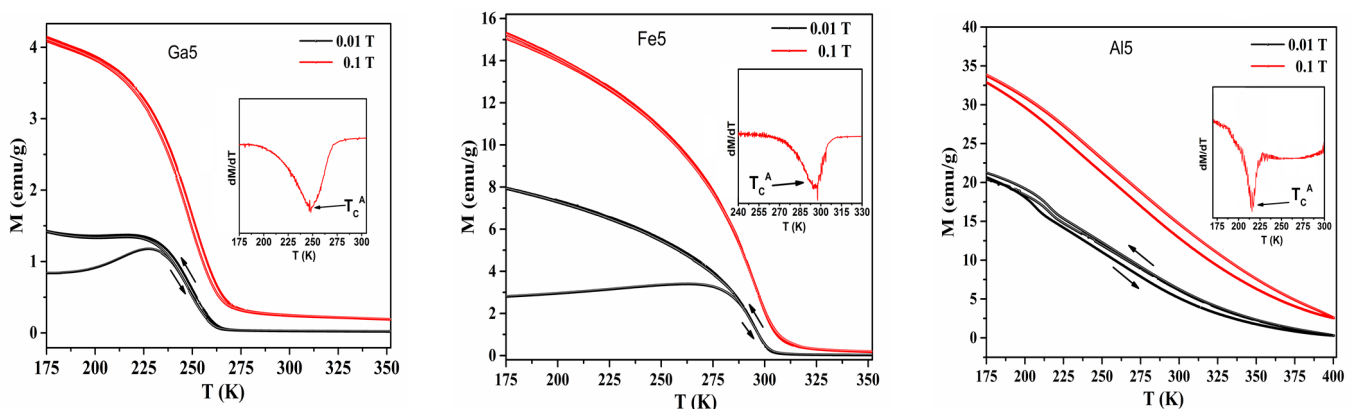


Figure 3. Typical SEM micrographs of wheel surfaces for different studied ribbons and EDX microanalysis.

The magnetization,  $M(T)$ , and its temperature dependence are shown in Figure 4 for external magnetic fields of 0.01 T (black curves) and 0.1 T (red curves). The analysis of this figure also confirms that the magnetic response (Curie temperature, magnetization) of the produced specimens is highly dependent on the minor addition of the fourth element. The minimum in the  $dM/dT$  vs. temperature graph, as illustrated by the inset in Figure 4, was used to determine the Curie temperature. The sharp peak indicates the occurrence of a martensitic transition at high temperatures. Additionally, austenite exhibits a ferromagnetic transition at  $T_C$  above its martensitic transition temperature. As seen in other Mn-rich Ni-Mn-Z martensitic alloys [25], martensite has relatively modest magnetization, much lower than that of FM austenite. This suggests that AFM coupling is prevalent in martensite. We can note that for the Al5 alloy, the FM to paramagnetic (PM) transition occurs at  $T_C = 220$  K, and for the Ga5 sample, this transition occurs at 252 K, while the Fe5 alloy displays the magnetic transition at  $T_C = 298$  K. The field-induced FM component in the austenite phase can be used for identifying this change in  $T_C$ . One possible explanation for the MT is the collective Jahn–Teller effect and, therefore, the density of electronic states at the Fermi level (NF) [12]. Thus, the temperature of the MT may rise as a result of the increase in NF brought on by applied magnetic fields. However, all examined ribbons exhibited the normal ferromagnetic characteristic of decreasing magnetism with temperature. The Ga5 alloy exhibited a reduction in magnetization and thermal hysteresis at a low magnetic field (0.01 T), which is brought on by the magnetic transition from FM to PM state near the  $T_C$  point. It should be emphasized that hysteretic behavior can be caused by a number of magnetic phenomena connected to high magnetic shape anisotropy or domain structure. In order to reduce the impact of a low magnetic field, the  $M(T)$  curves were measured under a

strong magnetic field (0.1 T). Nevertheless, in the case of the Fe5 alloy, we can observe a steady decrease in magnetization with similar hysteresis behavior at low magnetic fields (0.01 T), whereas at magnetic fields of 0.1 T, no features typical of the FM/PM transition were observed. This may be because there is a significant difference between the metallic radii of Fe (126 pm) and In (166 pm), which may be one possible explanation for this change. Also, the obtained maximum values of magnetization were found to be 1.5 emu/g (Ga 5) and 2.6 emu/g (Fe 5) at a low magnetic field of 0.01 T. These results are equivalent to those obtained above the structural phase transition from a PM martensitic state to a PM austenitic state for the Heusler  $\text{Ni}_{50}\text{Mn}_{36.5}\text{In}_{13.5}$  alloy (0.6 emu/g, at 0.01 T) [26]. We could deduce from the austenite phase's low magnetization value that it stays in the PM state at low magnetic fields at all temperatures over TM. As a result, the austenite phase's hypothetical  $T_C$  is only a little below TM.



**Figure 4.** Temperature dependence of the magnetization measured at magnetic fields 0.01 T and 0.1 T for studied alloys. The insets show the corresponding  $dM/dT(T)$  curves, which clearly indicate the transformation temperatures. Arrows indicate heating or cooling curves.

At magnetic fields smaller than 1 T, we can observe that the MT temperatures,  $T_A$ , and  $T_M$  are almost constant, which is consistent with the literature [27]. Another situation can be seen in the case of the Al5 alloy, a steady decrease in magnetization with hysteretic behavior comparable to that of a weak magnetic field. In contrast, the thermodynamic hysteresis was not detected when  $M(T)$  was measured in a high magnetic field (0.1 T). As a result, the domain structure in weak magnetic fields or strong magnetic anisotropy may be to blame for the hysteretic behavior, which is consistent with observations by other authors [28].

The isothermal magnetization curves  $M(H)$  as a function of the applied magnetic field up to 5 T around  $T_C$  are shown in Figure 5.

In the  $M(H)$  curves at low temperatures, the ferromagnetic behavior in the ground state may be observed. While the magnetization of the Al5 ribbon alloy reached saturation at a magnetic field of 5 T, that of the Ga5 and Fe5 alloys did not reach saturation until a magnetic field of 5 T. These curves demonstrate a notable magnetization change around the  $T_C$ . It implies that the FM/PM transition temperature, which occurred at  $T_C$ , may have been coupled with a significant shift in magnetic entropy. The magnetic entropy change ( $\Delta S_M$ ) is related to the MCE in the magnetic system, which can be caused by an applied magnetic field that causes a change in the magnetic order.

Based on the isothermal magnetization  $M(H)$  curves and by using the Maxwell relation [29], the magnetic entropy change ( $\Delta S_M$ ) was determined. The Ga5, Fe5, and Al5 alloys subjected to magnetic field variations up to 5 T are shown in Figure 6 to exhibit the variation in  $-\Delta S_M$  as a function of temperature.

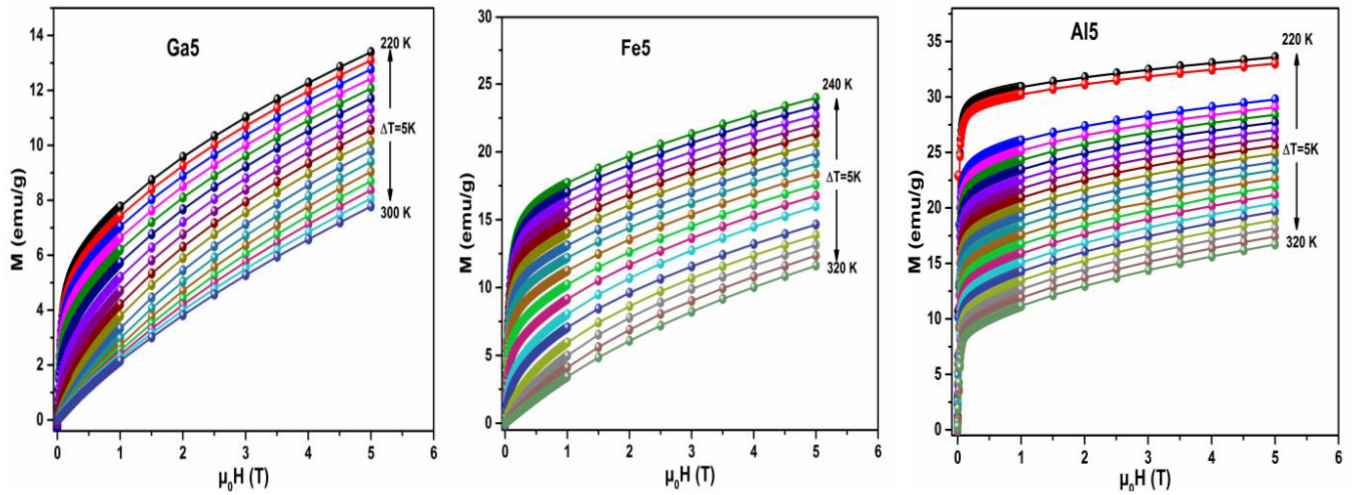


**Figure 5.** Isothermal magnetization (Ga5, Ge5 and Al5 alloys) around the Curie temperatures at different temperatures.

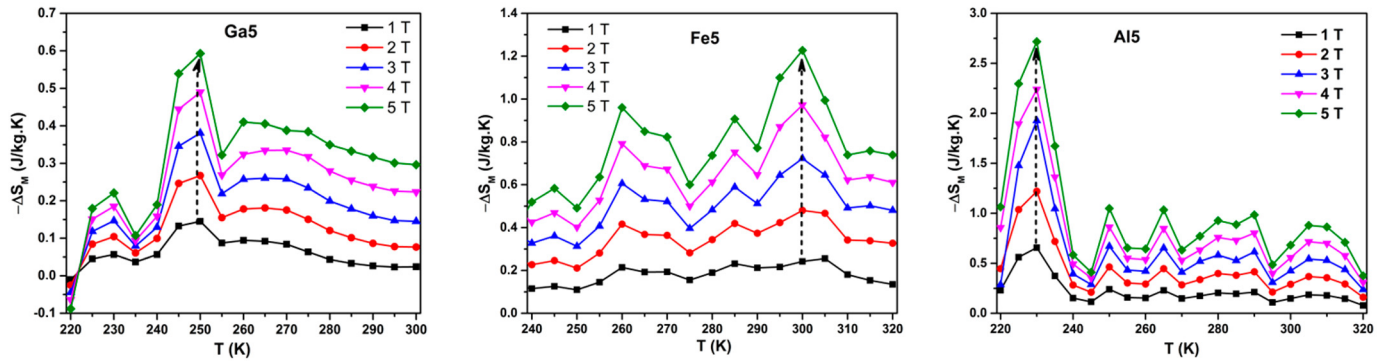


**Figure 6.**  $-\Delta S_M(T)$  curves for Ga5, Fe5, and Al5 alloys under magnetic field changes up to 5 T.

We can see that near  $T_C$ , the maximum magnetic entropy change,  $-(\Delta S_M)_{max}$ , rises with increasing applied magnetic field and reaches 0.59 J/kg K for the Ga5 alloy, 1.23 J/kg K for the Fe5 sample, and 2.71 J/kg K for the Al5 alloy (see Figure 7, for  $\mu_0\Delta H = 5$  T). It should be noted that the general trend of the increase in the maximum magnetic entropy change versus  $\mu_0\Delta H$  is linear.

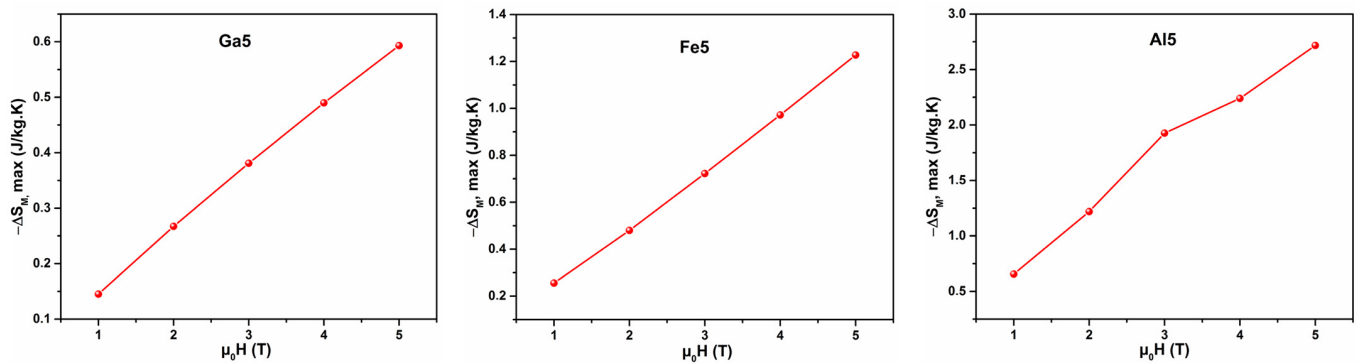


**Figure 7.** The corresponding magnetic field dependence of  $-(\Delta S_M)_{max}$  for the studied Ga5, Fe5, and Al5 alloys.

The obtained values for these alloys are equivalent to other magnetocaloric and Heusler alloys, such as  $Ni_{50}Mn_{35}In_{14}Bi_1$  ribbons (0.5 J/kg K for  $\mu_0\Delta H = 5$  T) [22],

$\text{Ni}_{50}\text{Mn}_{30}\text{In}_{20}$  ribbons (2.05 J/kg K for  $\mu_0\Delta H = 5$  T) [29],  $\text{Ni}_{50}\text{Mn}_{35}\text{In}_{13.5}\text{Bi}_{1.5}$  ribbons (0.2 J/kg K for  $\mu_0\Delta H = 5$  T) [22],  $\text{Ni}_{50}\text{Mn}_{30}\text{Sn}_{20}$  ribbons (2.43 J/kg K for  $\mu_0\Delta H = 5$  T) [29], and  $\text{Ni}_{50}\text{Mn}_{34}\text{In}_{14}\text{Ga}_2$  bulk (4 J/kg K for  $\mu_0\Delta H = 5$  T) [30].

From the abovementioned, we can note that these studied alloys have the potential to be used as novel magnetocaloric materials. Particularly, doping Al in the In sites is much better than doping Ga or Fe in the same sites, which increases the full-width-at-half-maximum ( $\Delta T_{\text{FWHM}}$ ) of the  $-\Delta S_M$  curve at  $T_C$ , hence improving the refrigeration capacity (RC). To assess the magnetocaloric properties of these alloys, the RC is one more significant factor, which is determined by the equation details in the following reference [31]. With the increase in a magnetic field up to 5 T, the RC increases linearly, and large values of RC are acquired with these alloys. The maximum RC in the vicinity of  $T_C$  under an applied field of  $\Delta H = 5$  T was found to be 25.72 J/kg (Ga5), 74.38 J/kg (Fe5), and 98.01 J/kg (Al5), as shown in Figure 8. These are typical figures for materials that are candidates for magnetic refrigeration systems because the refrigeration capacity is an indicator of the energy that can be removed by cooling, and the magnetocaloric effect is at maximum close to the Curie temperature. Likewise, the results of this work confirm the high influence of the minor addition of a fourth element on the functional response.

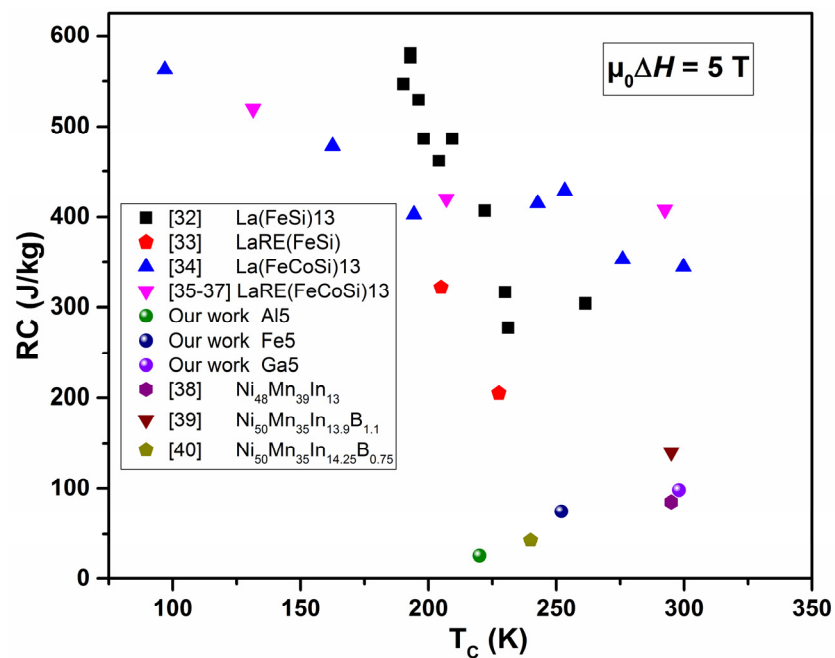


**Figure 8.** Relationship between RC and  $T_C$  at  $\mu_0\Delta H = 5$  T for different alloys (data taken from this work (Al5, Fe5, Ga5) and from references [32–40]).

The calculated values of RC are comparable to those of rare-earth-based systems near RT [32–37]. Also, these values are comparable to those of Heusler alloy ribbons such as  $\text{Ni}_{50}\text{Mn}_{35}\text{In}_{13.9}\text{B}_{1.1}$  (140 J/kg with  $\Delta H = 5$  T) [38],  $\text{Ni}_{50}\text{Mn}_{35}\text{In}_{14.25}\text{B}_{0.75}$  (43 J/kg with  $\Delta H = 5$  T) [39], and  $\text{Ni}_{48}\text{Mn}_{39}\text{In}_{13}$  (85 J/kg with  $\Delta H = 5$  T) [40]. Thus, the obtained RC and  $\Delta S_M$  values close to  $T_C$  make these studied alloys attractive as potential magnetic refrigerant materials, observing the interest of studies linked to the minor addition of elements to Ni-Mn-In based Heusler alloys [41]. As a result, Al doping induces chemical pressure and disorder, provoking an enrichment of MCE under an applied magnetic field of 5 T. These observations point to the possibility of this material being used as a solid refrigerant in the future, able to be introduced in magnetic refrigeration devices as an alternative to conventional gas-compression refrigeration devices. Magnetic refrigeration is an eco-friendly technology.

#### 4. Conclusions

In summary, structural, magnetocaloric, and magnetic measurements were carried out on  $\text{Ni}_{50}\text{Mn}_{35}\text{In}_{10}\text{X}_5$  ( $X = \text{Ga}, \text{Fe}, \text{or Al}$ ) under magnetic fields up to 5 T. All ribbons exhibited a mixture of cubic  $L2_1$  and tetragonal  $L1_0$  structure and underwent second-order magnetic transitions at 220 K, 252 K, and 298 K for Al5, Ga5, and Fe5, respectively.  $M(T)$  dependences exhibited a thermal hysteresis at saturation magnetic fields, indicating the presence of the structural change for the Ga5 alloy. The reduction in magnetization at a low magnetic field (0.01 T) accompanied thermal hysteresis, which is brought on at the  $T_C$  point by the magnetic transition from the FM to the PM state. In contrast, the Fe5 alloy showed a gradual loss of magnetization and similar hysteresis behavior at low magnetic fields (0.01 T), whereas at high magnetic fields (0.1 T), no features corresponding to the FM/PM transition were observed. This may be because there is a significant difference between the metallic radii of Fe and In. Moreover, the structural transformation temperature and  $T_C$  may be shifted to low temperatures if In is replaced with Al, according to magnetic measurements. Indeed, chemical composition has a significant impact on both the temperature of structural change and the transition itself. The  $\Delta S_M$  curves showed a narrow temperature range at  $T_C$ , resulting in values of RC for the Ga5, Fe5, and Al5 alloys of around 25 J/kg, 74 J/kg, and 98 J/kg, respectively. These materials are possible contenders for multifunctional applications because of the good physical characteristics displayed during the MT that takes place close to RT and their affordable cost.

**Author Contributions:** Conceptualization, J.-J.S. and W.R.; formal analysis, R.C., T.B. and J.S.; investigation, T.B.; writing—original draft, T.B.; writing—review and editing, T.B. and J.-J.S. All authors have read and agreed to the published version of the manuscript.

**Funding:** The Independent Research and Development Project of Shanghai Key Laboratory of Advanced Ferrometallurgy, Shanghai University (SKLASS 2020-Z07), and PONT2020/01 from the University of Girona all provided funding for this work.

**Data Availability Statement:** Data available by requesting the corresponding authors.

**Conflicts of Interest:** The authors declare no conflict of interest.

#### References

1. Bachaga, T.; Zhang, J.; Khitouni, M.; Suñol, J.J. NiMn-based Heusler magnetic shape memory alloys: A review. *Int. J. Adv. Manuf. Technol.* **2019**, *103*, 2761–2772. [[CrossRef](#)]
2. Zhang, R.; Sun, D.; Ji, C.; Chen, Y.; Zhang, X.; Dong, Z. Shape memory effect and martensitic transformation in Fe–Mn–Al–Ni Alloy. *Metals* **2022**, *12*, 247. [[CrossRef](#)]
3. Liao, X.Q.; Wang, Y.; Wetterskog, E.; Cheng, F.; Hao, C.X.; Khan, M.T.; Zheng, Y.Z.; Yang, S. Superposition of conventional and spontaneous exchange bias in a  $\text{Ni}_{50}\text{Mn}_{34}\text{In}_{13}\text{Fe}_3$  magnetic shape memory alloy. *J. Alloys Comp.* **2019**, *772*, 988–993. [[CrossRef](#)]
4. Marchenkov, V.V.; Emelyanova, S.M.; Marchenkova, E.B. Martensitic transformation temperatures and Hall effect in  $\text{Ni}_{47-x}\text{Mn}_{41+x}\text{In}_{12}$  ( $x = 0, 1, 2$ ) Alloys. *Materials* **2023**, *16*, 672. [[CrossRef](#)] [[PubMed](#)]
5. Tavares, S.; Yang, K.; Meyers, M.A. Heusler alloys: Past, properties, new alloys, and prospects. *Prog. Mater. Sci.* **2023**, *132*, 101017. [[CrossRef](#)]
6. Konoplyuk, S.; Kolomiets, A.; Prokleska, J.; Proschek, P.; Buturlim, V.; Gerstein, G.; Jürgen Maier, H. Pressure and magnetic field-induced transport effects in  $\text{Ni}_{45.4}\text{Mn}_{40}\text{In}_{14.6}$  alloy. *Phys. Scr.* **2021**, *96*, 125833. [[CrossRef](#)]
7. Bachaga, T.; Daly, R.; Escoda, L.; Suñol, J.J.; Khitouni, M. Influence of chemical composition on martensitic transformation of MnNiIn shape memory alloys. *J. Therm. Anal. Cal.* **2015**, *122*, 167–173. [[CrossRef](#)]
8. Sivaprakash, P.; Kim, I.; Divya, S.; Hajra, S.; Hwan Oh, T.; Esakki Muthu, S. Influence of non-magnetic Cu on structural, magnetic and magnetocaloric properties on NiMnIn bulk Heusler alloys. *Mater. Sci. Eng. B* **2023**, *297*, 116760. [[CrossRef](#)]
9. Blinov, M.; Aryal, A.; Pandey, S.; Dubenko, I.; Talapatra, S.; Prudnikov, V.; Lähderanta, E.; Stadler, S.; Buchelnikov, V.; Sokolovskiy, V.; et al. Effects of magnetic and structural phase transitions on the normal and anomalous Hall effects in Ni–Mn–In–B Heusler alloys. *Phys. Rev. B* **2020**, *101*, 094423. [[CrossRef](#)]
10. Pathak, A.K.; Dubenko, I.; Karaca, H.E.; Stadler, S.; Ali, N. Large inverse magnetic entropy changes and magnetoresistance in the vicinity of a field-induced martensitic transformation in  $\text{Ni}_{50-x}\text{Co}_x\text{Mn}_{32-y}\text{Fe}_y\text{Ga}_{18}$ . *Appl. Phys. Lett.* **2010**, *97*, 450. [[CrossRef](#)]
11. Krenke, T.; Acet, M.; Wassermann, E.F.; Moya, X.; Vila, A.P. Ferromagnetism in the austenitic and martensitic states of Ni–Mn–In alloys. *Phys. Rev. B* **2006**, *73*, 174413. [[CrossRef](#)]

12. Suñol, J.J.; Escoda, L.; Hernando, B.; Llamazares, J.L.S.; Prida, V.M. Structural behavior of Ni-Mn-(In, Sn) Heusler melt spun ribbons. *EDP Sci.* **2009**, 02031. [[CrossRef](#)]
13. Bachagha, T.; Ren, W.; Suñol, J.J.; Jing, C. Microstructure characterization, structure and magnetic properties of Ni-Mn-Sn shape memory alloys. *J. Therm. Anal. Cal.* **2022**, *147*, 2147–2154. [[CrossRef](#)]
14. Bachagha, T.; Suñol, J.J. All-*d*-metal Heusler alloys: A review. *Metals* **2023**, *13*, 111. [[CrossRef](#)]
15. Llamazares, J.; Sanchez, T.; Santos, J.D.; Perez, M.J.; Sanchez, M.L.; Hernando, B.; Escoda, L.; Suñol, J.J.; Varga, R. Martensitic phase transformation in rapidly solidified Mn<sub>50</sub>Ni<sub>40</sub>In<sub>10</sub> alloy ribbons. *Appl. Phys. Lett.* **2008**, *92*, 4358.
16. Yan, F.; Yuan, X.; Zhou, M.; Gao, L. Improvement of mechanical properties and magnetocaloric effect in Ag doped Ni-Mn-In magnetic shape memory alloys. *J. Alloys Comp.* **2023**, *944*, 169143.
17. Camarillo-Garcia, J.P.; Hernández-Navarro, P.; Flórez-Zúñiga, H.; Baltazar-Hernández, V.H.; Alvarado-Hernández, F. Contrasting response on magnetocaloric effect and refrigeration capacity due to Ni or Mn substitution by Fe in Ni-Mn-In-Co-Fe alloy. *J. Alloys Comp.* **2022**, *934*, 167852. [[CrossRef](#)]
18. Feng, Y.; Gao, J.; Zhou, M.; Wang, H. Giant magnetocaloric effect induced by lower stress in Ni-Mn-In-Fe ferromagnetic shape memory alloys. *J. Magn. Magn. Mater.* **2022**, *563*, 169906. [[CrossRef](#)]
19. Lutterotti, L.; Matthies, S.; Wenk, H. MAUD: A friendly Java program for material analysis using diffraction. *IUCr Newsl. CPD* **1999**, *21*, 14–15.
20. Zhang, C.L.; Shi, H.F.; Ye, E.J.; Nie, Y.G.; Han, Z.D.; Qian, B.; Wang, D.H. Magnetostructural transition and magnetocaloric effect in MnNiSi-Fe<sub>2</sub>Ge system. *Appl. Phys. Lett.* **2015**, *107*, 020401–020439. [[CrossRef](#)]
21. Chen, J.H.; Trigg, A.; Chhetri, T.P.; Young, D.P.; Stadler, S. The influence of Au substitution and hydrostatic pressure on the phase transitions and magnetocaloric properties of MnCoGe alloys. *J. Appl. Phys.* **2020**, *127*, 213901. [[CrossRef](#)]
22. Aryal, A.; Quetz, A.; Pandey, S.; Dubenko, I.; Stadler, S.; Ali, N. Effect of Bi substitution on the magnetic and magnetocaloric properties of Ni<sub>50</sub>Mn<sub>35</sub>In<sub>15-x</sub>Bi<sub>x</sub> Heusler alloys. *AIP Adv.* **2017**, *8*, 056409. [[CrossRef](#)]
23. Pathak, A.K.; Khan, M.; Gautam, B.R.; Stadler, S.; Dubenko, I.; Ali, N. Exchange bias in bulk Ni-Mn-In-based Heusler alloys. *J. Magn. Magn. Mater.* **2009**, *321*, 963–965. [[CrossRef](#)]
24. Quetz, A.; Mucharla, B.; Samanta, T.; Dubenko, I.; Talapatra, S.; Stadler, S.; Ali, N. Phase diagram and magnetocaloric effects in Ni<sub>50</sub>Mn<sub>35</sub>(In<sub>1-x</sub>Cr<sub>x</sub>)<sub>15</sub> and (Mn<sub>1-x</sub>Cr<sub>x</sub>)NiGe<sub>1.05</sub> alloys. *J. Appl. Phys.* **2014**, *115*, 4722. [[CrossRef](#)]
25. Chen, J.; Bruno, N.M.; Karaman, I.; Huang, Y.; Li, J.; Ross, J., Jr. Direct measure of giant magnetocaloric entropy contributions in Ni-Mn-In. *J. Alloys Compds.* **2016**, *105*, 176–181. [[CrossRef](#)]
26. Pathak, A.K.; Dubenko, I.; Pueblo, C.; Stadler, S.; Ali, N. Magnetoresistance and magnetocaloric effect at a structural phase transition from a paramagnetic martensitic state to a paramagnetic austenitic state in Ni<sub>50</sub>Mn<sub>36.5</sub>In<sub>13.5</sub> Heusler alloys. *Appl. Phys. Lett.* **2010**, *96*, 945. [[CrossRef](#)]
27. Llamazares, J.; Flores-Zuiga, H.; Sánchez-Valdes, C.; Ross, C.; García, C. Refrigerant capacity of austenite in as-quenched and annealed Ni<sub>51.1</sub>Mn<sub>31.2</sub>In<sub>17.7</sub> melt spun ribbons. *J. Appl. Phys.* **2012**, *111*, 927–932.
28. Mha, B.; Lgb, C.; Rvb, C. Study of martensitic transition temperature on Ni<sub>54</sub>Fe<sub>19</sub>Ga<sub>23</sub>X<sub>4</sub> Heusler glass-coated microwires doped by X = B, Al, Ga, In. *J. Magn. Magn. Mater.* **2022**, *542*, 168605.
29. Caron, L.; Ou, Z.Q.; Nguyen, T.T.; Thanh, D.; Tegus, O.; Brück, E. On the determination of the magnetic entropy change in materials with first-order transitions. *J. Magn. Magn. Mater.* **2009**, *321*, 3559–3566. [[CrossRef](#)]
30. Aksoy, S.; Krenke, T.; Acet, M.; Wassermann, E.F.; Moya, X.; Manosa, L.; Planes, A. Tailoring magnetic and magnetocaloric properties of martensitic transitions in ferromagnetic Heusler alloys. *Appl. Phys. Lett.* **2007**, *91*, 241916. [[CrossRef](#)]
31. Gschneidner, Jr., K.A.; Pecharsky, V.K.; Tsokol, A.O. Recent developments in magnetocaloric materials. *Rep. Prog. Phys.* **2005**, *68*, 1479–1539. [[CrossRef](#)]
32. Jia, L.; Sun, J.R.; Shen, J.; Dong, Q.Y.; Zou, J.D.; Gao, B.; Zhao, T.Y.; Zhang, H.W.; Hu, F.X.; Shen, B.G. Magnetocaloric effects in the La(Fe,Si)<sub>13</sub> intermetallics doped by different elements. *J. Appl. Phys.* **2009**, *105*, 3675. [[CrossRef](#)]
33. Zhang, H.; Long, Y.; Cao, Q.; Zou, M.; Gschneidner, K.A.; Pecharsky, V.K. Effect of Ca on the Microstructure and Magnetocaloric Effects in the La<sub>1-x</sub>Ca<sub>x</sub>Fe<sub>11.5</sub>Si<sub>1.5</sub> Compounds. *Chem. Inform.* **2011**, *42*, 3746–3750. [[CrossRef](#)]
34. Zhang, H.; Shen, J.; Xu, Z.; Zheng, X.; Hu, F.; Sun, J.; Shen, B. Simultaneous enhancements of Curie temperature and magnetocaloric effects in the La<sub>1-x</sub>Ce<sub>x</sub>Fe<sub>11.5</sub>Si<sub>1.5</sub>C<sub>y</sub> compounds. *J. Magn. Magn. Mater.* **2012**, *324*, 484–487. [[CrossRef](#)]
35. Patissier, A.; Paul-Boncour, V. Fast synthesis of LaFe<sub>13-x</sub>Si<sub>x</sub> magnetocaloric compounds by reactive Spark Plasma Sintering. *J. Alloy Compds.* **2015**, *645*, 143–150. [[CrossRef](#)]
36. Balli, M.; Fruchart, D.; Gignoux, D. Optimization of La(Fe,Co)<sub>13-x</sub>Si<sub>x</sub> based compounds for magnetic refrigeration. *J. Phys. Cond. Matt.* **2007**, *19*, 236230. [[CrossRef](#)]
37. Kumar, P.; Lyubina, J.; Gutfleisch, O. Magnetic and magnetocaloric effect in melt spun La<sub>1-x</sub>R<sub>x</sub>Fe<sub>13-y</sub>Al<sub>y</sub>C<sub>z</sub> (R = Pr and Nd) compounds. *J. Phys. D* **2009**, *42*, 205003–205008. [[CrossRef](#)]
38. Pandey, S.; Quetz, A.; Aryal, A.; Dubenko, I.; Mazumdar, D. Magnetocaloric, thermal, and magnetotransport properties of Ni<sub>50</sub>Mn<sub>35</sub>In<sub>13.9</sub>B<sub>1.1</sub> Heusler alloy. *J. Magn. Magn. Mater.* **2017**, *444*, 98–101. [[CrossRef](#)]
39. Pandey, S.; Quetz, A.; Ibarra-Gaytan, P.J.; Sánchez-Valdés, C.F.; Aryal, A.; Dubenko, I.; Sanchez Llamazares, J.L.; Stadler, S.; Ali, N. Magnetostructural transitions and magnetocaloric effects in Ni<sub>50</sub>Mn<sub>35</sub>In<sub>14.25</sub>B<sub>0.75</sub> ribbons. *AIP Adv.* **2018**, *8*, 056434. [[CrossRef](#)]

40. Zhao, X.G.; Hsieh, C.C.; Lai, J.H.; Cheng, X.J.; Chang, W.C.; Cui, W.B.; Liu, W.; Zhang, Z.D. Effects of annealing on the magnetic entropy change and exchange bias behavior in melt-spun Ni–Mn–In ribbons. *Scr. Mater.* **2010**, *63*, 250–253. [[CrossRef](#)]
41. Venkatesan, S.; Kavita, S.; Perumal, S. Structure stability driven large magnetocaloric response in Ni-Co-Mn-In-Si Heusler alloy. *Ceram. Int.* **2022**, *48*, 29059–29066. [[CrossRef](#)]

**Disclaimer/Publisher’s Note:** The statements, opinions and data contained in all publications are solely those of the individual author(s) and contributor(s) and not of MDPI and/or the editor(s). MDPI and/or the editor(s) disclaim responsibility for any injury to people or property resulting from any ideas, methods, instructions or products referred to in the content.